

Rate response of neurons subject to fast or frozen noise: From stochastic and homogeneous to deterministic and heterogeneous populations

Azadeh Khajeh Alijani and Magnus J. E. Richardson*

*Mathematics Institute, University of Warwick, CV4 7AL, United Kingdom and
Warwick Systems Biology Centre, University of Warwick, CV4 7AL, United Kingdom*

(Received 4 May 2011; published 25 July 2011)

The response of a neuronal population to afferent drive can be expected to be sensitive to both the distribution and dynamics of membrane voltages within the population. Voltage fluctuations can be driven by synaptic noise, neuromodulators, or cellular inhomogeneities: processes ranging from millisecond autocorrelation times to effectively static or “frozen” noise. Here we extend previous studies of filtered fluctuations to the experimentally verified exponential integrate-and-fire model. How fast or frozen fluctuations affect the steady-state rate and firing-rate response are both examined using perturbative solutions and limits of a $1 + 2$ dimensional Fokker-Planck equation. The central finding is that, under conditions of a more-or-less constant population voltage variance, the firing-rate response is only weakly dependent on the fluctuation filter constant: The voltage distribution is the principal determinant of the population response. This result is unexpected given the nature of the systems underlying the extreme limits of fast and frozen fluctuations; the first limit represents a homogeneous population of neurons firing stochastically, whereas the second limit is equivalent to a heterogeneous population of neurons firing deterministically.

DOI: [10.1103/PhysRevE.84.011919](https://doi.org/10.1103/PhysRevE.84.011919)

PACS number(s): 87.19.1l, 87.19.1c, 87.19.1q, 87.85.dm

I. INTRODUCTION

Neurons *in situ* are subject to fluctuations arising from a variety of biophysical phenomena with intrinsic correlation times spanning a wide range: fast excitatory AMPA and inhibitory GABA_A synapses at the 1–10 millisecond time scale; slow excitatory NMDA and inhibitory GABA_B synapses at 10–100 of milliseconds; neuromodulators such as acetylcholine, dopamine, and adenosine acting on time scales of minutes or longer; and static fluctuations or “frozen noise” that arise, for example, from the range of resting potentials of neurons within an inhomogeneous population.

The resulting distribution and dynamics of membrane voltages within a population of neurons are likely to have a significant effect on its response to afferent synaptic drive. A number of theoretical studies have analyzed the dependency of the firing rate on filtered fluctuations using the leakless and leaky integrate-and-fire (LIF) models in both the fast and slow limits [1–6] and the quadratic integrate-and-fire (QIF) model [7] that features a spike and reset to minus infinity [8]. One motivation of these studies was to evaluate to what extent the steady-state firing rates derived in the analytically convenient limit of white-noise fluctuations approximated the more biophysically realistic case of synaptic filtering at AMPA (2 ms) or GABA_A (10 ms) time scales. Leading-order corrections to the white-noise limit were derived for the steady-state rate and shown to differ qualitatively for the LIF model $\sim \sqrt{\tau_s/\tau_v}$ [1,5] and the QIF model $\sim \tau_s/\tau_v$ [8], where τ_s is the filter time constant and τ_v the membrane time constant. The different scalings arise from the distinct ways fluctuations interact with the discontinuous, low threshold of the LIF or the smoother, parabolic threshold of the QIF, highlighting the singular nature of the LIF model

when compared to integrate-and-fire models with explicit spikes

The exponential integrate-and-fire (EIF) model [9] is in the same class of type-I neuron as the QIF and has been recently shown to provide an accurate reduced description of the response properties of neocortical layer-5 pyramidal cells [10] and fast-spiking interneurons [11]. In place of the parabolic spike-generating mechanism of the QIF model, the EIF neuron features an exponential term that models well the activation of the sodium current. This threshold is functionally sharper than the QIF and can capture the kinklike spikes seen *in vivo* [12]. The current-voltage relation of the EIF is, in some sense, intermediate between the LIF and the QIF, and additionally it provides an accurate reduced-model fit to experiment. It is therefore of interest technically and also from the point of incorporating further biological realism into an experimentally verified model, to analyze the firing-rate properties of the EIF neuron subject to fluctuating drive: This is the aim of this paper.

In Sec. II, the Fokker-Planck equation describing the EIF neuron driven by an Ornstein-Uhlenbeck (filtered white-noise process) is written in a form that allows for a perturbative solution in the limits of either fast or slow filtering. In Sec. III, solutions are provided for white, fast (weakly filtered), and frozen noise, adapting approaches previously developed for the QIF [8] and the LIF [6] steady-state rates. In Sec. IV the existing methodology is then generalized to the firing-rate response in the presence of filtered fluctuations, by considering how the instantaneous firing rate of a population of neurons is modulated by an oscillating current. As will be seen, under conditions of similar voltage distributions the steady-state rate and firing-rate response are surprisingly insensitive to the time scale of the filtering: The implication and scope of this result are considered in the Discussion in Sec. V. Finally, an appendix provides details of an efficient numerical scheme [13] that may be employed to calculate the various ratelike quantities derived in this paper.

*magnus.richardson@warwick.ac.uk

II. THE MODEL

A nonlinear integrate-and-fire neuron has a membrane voltage V driven by a zero-mean fluctuating variable S :

$$\tau_v \frac{dV}{dt} = F(V) + S, \quad (1)$$

$$\tau_s \frac{dS}{dt} = \sigma_v \sqrt{2(\tau_v + \tau_s)} \xi(t) - S. \quad (2)$$

In this paper the function $F(V)$, which is proportional to the ionic current, is taken to be that of the EIF model [9]. This function is parameterized by the equilibrium potential E , spike threshold V_T , and spike sharpness Δ_T :

$$F(V) = E - V + \Delta_T \exp[(V - V_T)/\Delta_T]. \quad (3)$$

A spike is registered when the voltage reaches V_{th} after which it is immediately reset to V_{re} . The limit $V_{\text{th}} \rightarrow \infty$ is taken in the analyses that follow. In the treatment of the QIF model [8] the reset was set at minus infinity. Unfortunately this is not possible for the EIF model, which requires a finite reset, complicating the analysis somewhat. Note that there is no reset or threshold for the fluctuating variable S .

Any tonic, conductance-based component [14] of the fluctuations has been absorbed into the definition of the voltage time constant τ_v , and the remaining fluctuations S are treated in the Gaussian approximation [15]. The zero-mean Gaussian white noise $\xi(t)$ is delta correlated $\langle \xi(t)\xi(t') \rangle = \delta(t-t')$ and has a prefactor chosen so that σ_v^2 would be the voltage variance in the absence of a spike-generating mechanism (for the case $V_T \rightarrow \infty$). The idea, therefore, is to examine the effect of synaptic filtering on the firing rate while keeping the voltage distribution roughly constant. This formulation differs slightly from that employed by Ref. [8] but has the advantage of lightening the analysis in the limit of frozen fluctuations.

Before giving the equations for a population of neurons it proves convenient to render the main quantities dimensionless by measuring time in units of τ_v and introducing the ratio $\kappa^2 = \tau_s/\tau_v$, by rescaling the voltage $v = (V - E)/\sigma_v$, and by rescaling the fluctuations $s\sigma_v = \sqrt{\kappa^2/(1 + \kappa^2)}$. In terms of these variables:

$$\frac{dv}{dt} = f(v) + \frac{s}{\kappa} \sqrt{1 + \kappa^2}, \quad (4)$$

$$\kappa^2 \frac{ds}{dt} = \sqrt{2\kappa^2} \xi(t) - s, \quad (5)$$

where $f(v) = \delta_T \exp[(v - v_T)/\delta_T] - v$ with v_T and δ_T being the appropriately scaled spike threshold and sharpness, and similarly for the reset potential v_{re} .

A. The Fokker-Planck equation

A population of neurons with dynamics obeying Eqs. (1) and (2) is considered, each receiving an independent realization of the fluctuating term $\xi(t)$. Standard methods [16] allow for a 1 + 2 dimensional Fokker-Planck equation to be written describing the evolution of the density $\mathcal{P}(v, s, t)$ of neurons with voltages near v and fluctuations near s . The continuity equation in terms of the voltage flux \mathcal{J}^v and fluctuation flux \mathcal{J}^s , with the reset boundary condition explicit, is

$$\partial_t \mathcal{P} + \partial_v \mathcal{J}^v + \partial_s \mathcal{J}^s = \mathcal{J}^{\text{th}} \delta(v - v_{\text{re}}), \quad (6)$$

where \mathcal{J}^{th} is \mathcal{J}^v evaluated in the limit $v \rightarrow \infty$. The fluxes obey

$$\begin{aligned} \mathcal{J}^v &= \left(f + \frac{s}{\kappa} \sqrt{1 + \kappa^2} \right) \mathcal{P}, \\ -\kappa^2 \mathcal{J}^s &= \partial_s \mathcal{P} + s \mathcal{P}. \end{aligned} \quad (7)$$

The instantaneous firing rate averaged across the population is $\mathcal{R}(t) = \int ds \mathcal{J}^{\text{th}}(s, t)$. The continuity and flux equations can be combined to yield the Fokker-Planck equation for the system

$$\begin{aligned} \mathcal{L}_s \mathcal{P} &= \kappa^2 \partial_t \mathcal{P} + \kappa \sqrt{1 + \kappa^2} \partial_v (s \mathcal{P}) \\ &\quad + \kappa^2 \partial_v [f \mathcal{P} - (f \mathcal{P})^{\text{th}} \theta(v - v_{\text{re}})]. \end{aligned} \quad (8)$$

The operator $\mathcal{L}_s = \partial_s^2 + \partial_s s$ has two solutions for $\mathcal{L}_s \phi = 0$ but only the even, Gaussian solution $\phi(s) = e^{-s^2/2}/\sqrt{2\pi}$ allows for normalizable probability densities. Note that $\phi(s)$ is also the marginal probability density for s . The following results will also be useful:

$$\mathcal{L}_s (s\phi) = -s\phi \quad \text{and} \quad \mathcal{L}_s (s^2\phi) = 2(1 - s^2)\phi. \quad (9)$$

The step function $\theta(v - v_{\text{re}})$ in Eq. (8) comes from moving the Dirac δ function in Eq. (6) under the voltage derivative, and $(f \mathcal{P})^{\text{th}} = \mathcal{J}^{\text{th}}$ comes from taking the limit $v_{\text{th}} \rightarrow \infty$ in the voltage flux Eq. (7).

Following Ref. [8] the Fokker-Planck Eq. (8) will be expanded in powers of κ to derive the first- and second-order corrections to the white-noise $\tau_s = 0$ limit. The equation has an invariance under simultaneous sign inversions of κ and s , which can be usefully exploited in the small- κ perturbation expansion:

$$\begin{aligned} \mathcal{P}(v, s, t; \kappa) &= \sum_{n=0}^{\infty} \kappa^n \mathcal{P}_n(v, s, t) = \mathcal{P}(v, -s, t; -\kappa) \\ &= \sum_{n=0}^{\infty} \kappa^n (-1)^n \mathcal{P}_n(v, -s, t), \end{aligned} \quad (10)$$

so that the n th component \mathcal{P}_n of the expanded probability density is an even function of s if n is an even integer (or equivalently odd). Because the firing rate $\mathcal{R}(t)$ involves an integral over s , a consequence of the even-odd symmetry is that there is no contribution to the firing rate at first order in κ (or any odd order).

The notational conventions are now illustrated using the probability density as an example; a calligraphic font $\mathcal{P}(v, s, t)$ denotes the full time-dependent quantity, a standard font $P(v, s)$ denotes the steady state, and a quantity with a hat $\hat{P}(v, s, \omega)$ is the complex, frequency-dependent amplitude of a sinusoidally modulated quantity [due to an oscillating afferent current $E \rightarrow E + \hat{E} e^{i\omega t}$ in Eq. (3)], so that the total probability density can be written $\mathcal{P} \simeq P + \hat{P} e^{i\omega t}$ for a weak modulation. Numerical subscripts denote the order of expansion, so P_n is the strength of the contribution at order κ^n to the steady-state probability density.

III. STEADY-STATE RATE

For the steady state the method used for the QIF [8] is followed, with differences arising from the finite reset condition, the exponential rather than quadratic spike, and the definition

of the fluctuation amplitude in Eq. (5). As it will be convenient to take moments with respect to powers of s of various quantities, the notation $\{s^m\} = \int ds s^m P(v, s)$ is introduced where $\{1\} = \int ds P(v, s)$ is the marginal distribution for the voltage. Integrating the continuity equation over s , substituting for J^v , and integrating voltage over $-\infty \rightarrow v$ yields

$$f\{1\} + \frac{\sqrt{1+\kappa^2}}{\kappa}\{s\} = R\theta(v - v_{re}), \quad (11)$$

where $R = \int ds J^{\text{th}}$ is the steady-state rate. Multiplying the Fokker-Planck Eq. (8) in the steady state by s and integrating over the full range of s yields

$$\{s\} = -\kappa\sqrt{1+\kappa^2}\partial_v\{s^2\} + \kappa^2\partial_v[f\{s\} - (f\{s\})^{\text{th}}\theta(v - v_{re})]. \quad (12)$$

Combining (11) and (12) yields the equation

$$R\theta(v - v_{re}) = f\{1\} - (1 + \kappa^2)\partial_v\{s^2\} - \kappa\sqrt{1+\kappa^2}\partial_v[f\{s\} - (f\{s\})^{\text{th}}\theta(v - v_{re})], \quad (13)$$

which is now used to derive the corrections to the density and rates order-by-order in κ .

A. Zeroth-order solution

The Fokker-Planck Eq. (8) at zero order in κ gives $\mathcal{L}_s P_0 = 0$ implying that the distribution factorizes $P_0(v, s) = \phi(s)Q_0(v)$, where $\phi(s)$ is the unit-variance Gaussian previously identified and $Q_0 = \{1\}_0$ is the marginal steady-state voltage distribution. From this, it must be that $\{s^2\}_0 = Q_0$ also, and so Eq. (13) yields

$$(f - \partial_v)Q_0 = R_0\theta(v - v_{re})$$

to give

$$Q_0 = R_0 \int_v^\infty dv' e^{-\int_v^{v'} dv'' f(v'')} \theta(v' - v_{re}), \quad (14)$$

which is the familiar form [9] for the white-noise case. The firing rate R_0 can be extracted by applying the normalization condition $\int dv Q_0 = 1$.

B. First-order solution

Equation (8) requires that $\mathcal{L}_s P_1 = s\partial_v P_0$. There can be no complementary function of the form $\phi(s)Q_1(v)$ to the solution of this equation because $P_1(v, s)$ is an odd function of s . So using result (9) the first-order density is $P_1 = -s\phi\partial_v Q_0$. Additionally, because P_1 is odd in s there is no contribution to the firing rate, so $R_1 = 0$.

C. Second-order solution

On evaluating Eq. (8) at order κ^2 , substituting for P_1 in terms of Q_0 , and making use of the differential Eq. (14) for Q_0 , the second-order Fokker-Planck equation reduces to $\mathcal{L}_s P_2 = (1 - s^2)\partial_v^2 P_0$. Applying the second result from equation set (9) gives a general solution of the form

$$P_2 = \phi Q_2 + \phi \frac{s^2}{2} \partial_v^2 Q_0. \quad (15)$$

It remains to derive an equation for the complementary solution $Q_2(v)$. The zero and second moments of Eq. (15) with respect to s are

$$\{1\}_2 = Q_2 + \frac{1}{2}\partial_v^2 Q_0 \quad \text{and} \quad \{s^2\}_2 = Q_2 + \frac{3}{2}\partial_v^2 Q_0. \quad (16)$$

So $\{1\}_2 = \{s^2\}_2 - \partial_v^2 Q_0$, which can be substituted into Eq. (13) evaluated at order κ^2 :

$$(f - \partial_v)\{s^2\}_2 = R_2\theta(v - v_{re}) + (\partial_v Q_0)(1 - \partial_v f) - \frac{R_0}{\delta_T}\delta(v - v_{re}), \quad (17)$$

where the results $\{s^2\}_0 = Q_0$, $\{s\}_1 = -\partial_v Q_0$, and $(f\partial_v Q_0)^{\text{th}} = -R_0/\delta_T$ in the limit $v_{\text{th}} \rightarrow \infty$ have all been used. This equation can be tidied up further by moving the Heaviside function and part of the Dirac delta function under the $(f - \partial_v)$ operator by using the relation $(f - \partial_v)Q_0 = R_0\theta(v - v_{re})$ and its voltage derivative. The resulting equation

$$(f - \partial_v)(\{s^2\}_2 - R_2 Q_0/R_0 + \partial_v Q_0/\delta_T) = \partial_v Q_0 - (\partial_v f)(\partial_v Q_0 + Q_0/\delta_T) \quad (18)$$

can be solved and integrated from $-\infty \rightarrow v$ to yield

$$\{s^2\}_2 = \frac{R_2}{R_0} Q_0 - \frac{\partial_v Q_0}{\delta_T} + \int_v^\infty dv' e^{-\int_v^{v'} du f(u)} \times \left[\partial_v Q_0 - \left(\partial_v Q_0 + \frac{Q_0}{\delta_T} \right) \partial_v f \right]. \quad (19)$$

The variance of s is unity and fully accounted for at zero order; therefore $\int dv \{s^2\}_2 = 0$. Using this result, and the facts that the full-range voltage integral of Q_0 is unity and the same integral of $\partial_v Q_0$ is zero, means that integrating (19) over voltage gives the second-order contribution to the steady-state rate R_2 as the double integral

$$R_0 \int_{-\infty}^\infty dv \int_v^\infty dv' e^{-\int_v^{v'} du f(u)} \left[\left(\partial_v Q_0 + \frac{Q_0}{\delta_T} \right) \partial_v f - \partial_v Q_0 \right]. \quad (20)$$

From the second of equation set (16) Q_2 can be found, which in turn yields the second-order contribution to the probability density

$$P_2 = \phi \left[\frac{R_2}{R_0} Q_0 - \frac{\partial_v Q_0}{\delta_T} + \frac{1}{2}(s^2 - 3)\partial_v^2 Q_0 \right] + \phi \int_v^\infty dv' e^{-\int_v^{v'} du f(u)} \left[\partial_v Q_0 - \left(\partial_v Q_0 + \frac{Q_0}{\delta_T} \right) \partial_v f \right]. \quad (21)$$

Threshold Integration [13] provides an efficient method for solving Eq. (17) or (18) numerically. In general this is a much more convenient way of arriving at the rate R_2 or the function $\{s^2\}_2$ than numerically evaluating the integrals (see the Appendix for details).

D. Limit of frozen fluctuations

Finally, the limiting result for $\kappa \rightarrow \infty$ will be derived following the method used in Ref. [6]. Starting with the

Fokker-Planck Eq. (8) and remembering that now κ^{-1} is the small parameter, the zero-order equation is

$$(s + f)P_\infty = (f P_\infty)^{\text{th}}\theta(v - v_{\text{re}}), \quad (22)$$

where, with a minor abuse of notation, the ∞ subscript corresponds to the case where $\kappa \rightarrow \infty$. The joint probability density can be written as $P_\infty(v, s) = P_\infty(v|s)\phi(s)$, where, because the fluctuations are effectively frozen from the point of view of the voltage variable, $P_\infty(v|s) = P_{\text{det}}$ is the voltage density for a deterministic neuron with constant input s obeying $\dot{v} = f(v) + s$. If s is below the critical value $s_c = v_T - \delta_T$ for the EIF model [9] the neuron does not fire and its density is the Dirac delta function $\delta(v - v_s)$, where v_s is the stable fixed point of the equation $s + f(v_s) = 0$. Above the critical drive s_c the probability density and firing rate R_{det} are

$$P_{\text{det}} = \frac{R_{\text{det}}\theta(v - v_{\text{re}})}{f + s} \quad \text{with} \quad R_{\text{det}} = \frac{1}{\int_{v_{\text{re}}}^{\infty} \frac{dv}{f+s}}. \quad (23)$$

Hence $(f P_\infty)^{\text{th}} = \theta(s - s_c)\phi(s)R_{\text{det}}$, and the firing rate in the frozen limit must be

$$R_\infty = \int_{-\infty}^{\infty} (f P_\infty)^{\text{th}} ds = \int_{s_c}^{\infty} ds \phi(s) R_{\text{det}}(s). \quad (24)$$

This form is intuitive because it represents a weighted average of deterministic firing rates over the distribution of s . It is identical to a form previously found for the LIF [6] and, as noted

in Ref. [17], also generalizes to non-Gaussian distributed frozen fluctuations. In this limit of slow noise, therefore, the original homogeneous, stochastic system becomes identical to a heterogeneous population of deterministic neurons, some of which are quiescent, whereas others are spiking regularly with a variety of fixed periods.

E. Summary for the steady state

The results for fast and slow fluctuations are compared for an example EIF model in Fig. 1. Figure 1(A) shows the steady-state firing rate for the white-noise [green line, Eq. (14)] and frozen-noise [red line, Eq. (24)] limits demonstrating a surprisingly close agreement for what are very different systems. The fast-noise expansion $R_0 + \kappa^2 R_2$, with $\tau_s = 2$ ms [black line, Eq. (20) for R_2], is also provided and compared to Monte Carlo simulations (black symbols). Two examples are chosen: (i) a suprathreshold-firing regime and (ii) a subthreshold-firing regime with the corresponding probability densities for the white and frozen limits provided as insets in the same panel. The agreement between the densities for the two limits in the subthreshold regime is a direct consequence of the choice of noise amplitude in Eq. (2) that ensures that the variance of the voltage is filter-constant independent as long as the voltage dynamics are not too strongly affected by the exponential term in Eq. (1). A similar argument for the suprathreshold regime accounts for why, in this case, there is more of a discrepancy

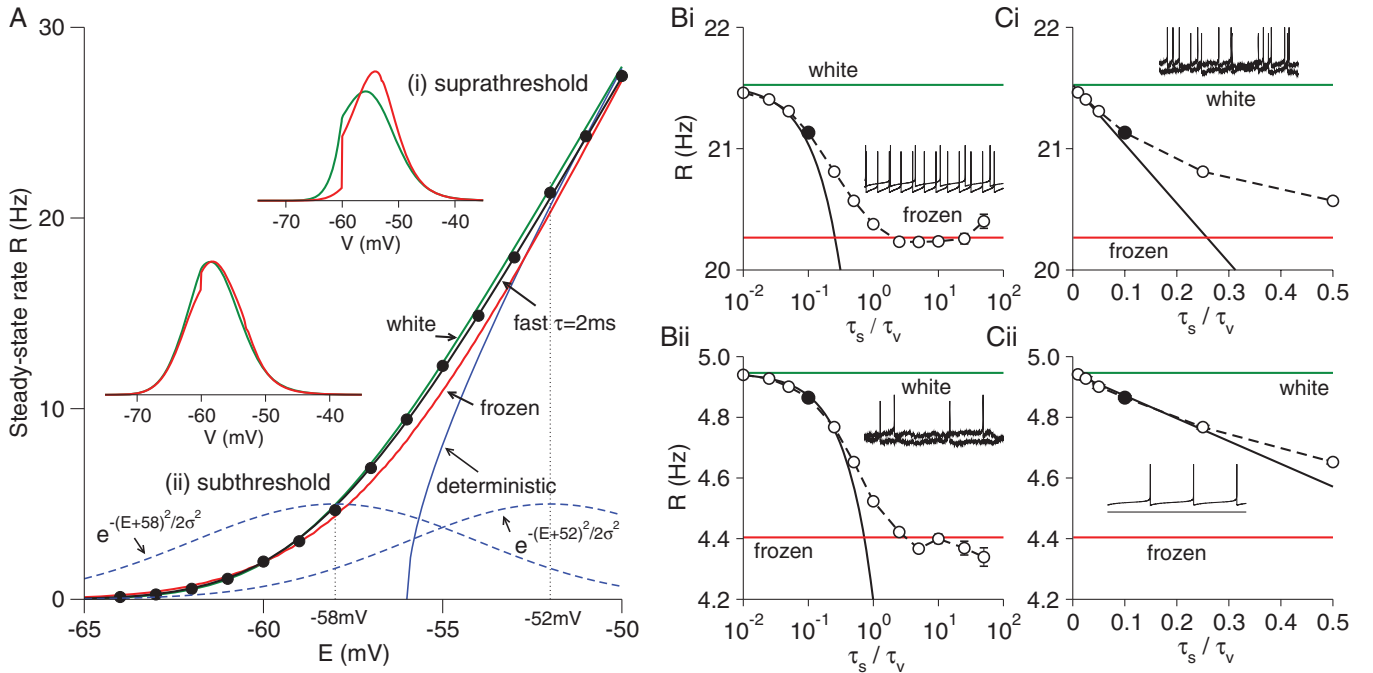


FIG. 1. (Color online) Steady state of the EIF model subject to filtered noise. (A) Steady-state rate for white-noise [green line, Eq. (14)], fast-noise expansion $R_0 + \kappa^2 R_2$ with $\tau_s = 2$ ms [black line, Eq. (20) for R_2], deterministic [blue line, Eq. (23)] and frozen-noise [red line, Eq. (24)] cases. Insets show the probability distributions for two example firing regimes: (i) suprathreshold with $E = -52$ mV and (ii) subthreshold with $E = -58$ mV for white and frozen limits. Note the discontinuity at $V = V_{\text{re}} = -60$ mV for the frozen-noise limits. The Gaussian distributions (blue dashed lines) correspond to ϕ used in Eq. (24) for the two examples. (Bi) The variation of the steady-state rate with the ratio τ_s/τ_v on a logarithmic scale for the suprathreshold firing regime example. (Ci) Detail of the same for small τ_s/τ_v on a linear scale. The fast-noise expansion (black line) is compared with simulations (symbols) and agrees well up to $\tau_s \simeq 2$ ms (black symbol). (Bii) and (Cii) Corresponding curves for the subthreshold firing regime example (ii). Insets to B and C show example voltage trajectories for white and frozen limits. Other parameters chosen were $\tau = 20$ ms, $V_{\text{re}} = -60$ mV, $V_{\text{th}} = 0$ mV, $\Delta_T = 3$ mV, $V_T = -53$ mV, and $\sigma = 4$ mV.

between the white and frozen limits: In this regime the neuron spends more time at depolarized voltages. It can be further noted that the densities for frozen noise (red curves) show jump discontinuities at $V = V_{re}$. This feature is also present in the fast-fluctuation expansion Eq. (21) in the derivative terms acting on Q_0 . The deterministic firing rate [blue line, Eq. (23)] and Gaussian distributions for the suprathreshold and subthreshold examples [blue dashed lines, $\phi(s)$ in Eq. (24)] used in the construction for the frozen rate Eq. (24) are also provided (the amplitudes are arbitrary).

Figures 1(b) and 1(c) examine the agreement between the second-order fast-fluctuation expansion (20) and Monte Carlo simulations for the suprathreshold and subthreshold firing-regime examples (i) and (ii). The expansion at this order is linear in the ratio of time constants $\kappa^2 = \tau_s/\tau_v$ and provides a good agreement when $\kappa^2 = 0.1$ corresponding to the scale $\tau_s = 2$ ms for fast AMPA excitatory synapses (black symbol). Simulations indicate that for the parameters chosen here the steady-state rates for slow filter constants become close to the frozen limit around $\tau_s \sim 10\tau_v$.

IV. FIRING-RATE RESPONSE

The firing-rate response to a weak sinusoidally modulated current is now considered by adding a term $\hat{\epsilon}e^{i\omega t}$ to the right-hand side of the scaled voltage Eq. (4). The linear response at the population level will feature induced modulations in the probability density $\mathcal{P} = P + \hat{P}e^{i\omega t}$ and the firing rate $\mathcal{R} = R + \hat{R}e^{i\omega t}$, where both \hat{P} and \hat{R} are proportional to $\hat{\epsilon}$. In the presence of white-noise analytical solutions to the firing-rate modulation have been derived for the leaky IF model [18] in terms of hypergeometric functions. For general nonlinear IF neurons analytical forms are not available; however, a Threshold Integration scheme [13] exists that provides exact numerical solutions for the modulated quantities in the presence of white noise. This integration scheme will now be generalized to the treatment of weakly filtered fluctuations. The approach is analogous to that taken for the steady state with the principal difference being that, at each order, there is an additional differential equation for the net voltage flux that needs to be solved simultaneously with the one for the probability density.

At the linear level in $\hat{\epsilon}$ the continuity equation for the amplitudes of the modulated probability densities and fluxes is

$$i\omega\hat{P} + \partial_v\hat{J}^v + \partial_s\hat{J}^s = \hat{J}^{\text{th}}\delta(v - v_{re}). \quad (25)$$

For a current modulation $\hat{\epsilon}e^{i\omega t}$ in Eq. (4) the corresponding flux equations, to linear order in $\hat{\epsilon}$, are

$$\hat{J}^v = \left(f + \frac{s}{\kappa}\sqrt{1 + \kappa^2}\right)\hat{P} + \hat{\epsilon}P \quad \text{and} \\ -\kappa^2\hat{J}^s = \partial_s\hat{P} + s\hat{P}. \quad (26)$$

Integrating the continuity equation and the voltage flux equations over s generates two equations coupled by the net voltage flux $\hat{J} = \int ds\hat{J}^v$:

$$\hat{R}\delta(v - v_{re}) = i\omega\{\hat{1}\} + \partial_v\hat{J}, \quad (27)$$

$$\hat{J} = f\{\hat{1}\} + \frac{\sqrt{1 + \kappa^2}}{\kappa}\{\hat{s}\} + \hat{\epsilon}\{1\}. \quad (28)$$

Note that at the analogous stage in the steady-state calculation Eq. (11) only one equation was required. Equations (25) and (26) together yield the modulated Fokker-Planck equation

$$\mathcal{L}_s\hat{P} = \kappa^2i\omega\hat{P} + \kappa\sqrt{1 + \kappa^2}\partial_v\hat{P} \\ + \kappa^2\partial_v[\hat{\epsilon}P + f\hat{P} - (f\hat{P})^{\text{th}}\theta(v - v_{re})] \quad (29)$$

from which the modulated moment $\{\hat{s}\}$ can be derived:

$$\{\hat{s}\} = -\kappa^2i\omega\{\hat{s}\} - \kappa\sqrt{1 + \kappa^2}\partial_v\{s^2\} \\ + \kappa^2\partial_v[\hat{\epsilon}\{s\} + f\{\hat{s}\} - (f\{\hat{s}\})^{\text{th}}\theta(v - v_{re})] \quad (30)$$

which can be substituted into (28)

$$\hat{J} = f\{\hat{1}\} + \hat{\epsilon}\{1\} - \kappa\sqrt{1 + \kappa^2}i\omega\{\hat{s}\} - (1 + \kappa^2)\partial_v\{s^2\} \\ - \kappa\sqrt{1 + \kappa^2}\partial_v[\hat{\epsilon}\{s\} + f\{\hat{s}\} - (f\{\hat{s}\})^{\text{th}}\theta(v - v_{re})]. \quad (31)$$

Equations (27), (29), and (31) are sufficient to generate pairs of equations that can be solved numerically order by order in κ .

A. Zeroth-order solution

The Fokker-Planck Eq. (29) at zero order in κ is $\mathcal{L}_s\hat{P}_0 = 0$ so $\hat{P}_0 = \phi\hat{Q}_0$ and from (27), (31)

$$\hat{R}_0\delta(v - v_{re}) = i\omega\hat{Q}_0 + \partial_v\hat{J}_0, \quad (32)$$

$$\hat{J}_0 = (f - \partial_v)\hat{Q}_0 + \hat{\epsilon}Q_0, \quad (33)$$

which are equivalent to the white-noise case [19] as expected and solvable by Threshold Integration [13] with details given in the Appendix.

B. First-order solution

From Eq. (29) the first-order solution obeys $\mathcal{L}_s\hat{P}_1 = s\partial_v\hat{P}_0$ and following similar arguments used for the steady state $\hat{P}_1 = -s\phi\partial_v\hat{Q}_0$.

C. Second-order solution

On substitution of \hat{P}_0 and \hat{P}_1 , the modulated Fokker-Planck equation at second order can be written

$$\mathcal{L}_s\hat{P}_2 = i\omega\phi\hat{Q}_0 + \phi\partial_v[f\hat{Q}_0 + \hat{\epsilon}Q_0 - \hat{R}_0\theta(v - v_{re})] \\ - s^2\phi\partial_v^2\hat{Q}_0. \quad (34)$$

The first four terms (those not proportional to s^2) also appear in the zeroth-order Eqs. (32) and (33). This allows Eq. (34) to be reduced to $\mathcal{L}_s\hat{P}_2 = (1 - s^2)\partial_v^2\hat{P}_0$ and so, following arguments used earlier for the steady state, $\hat{P}_2 = \phi\hat{Q}_2 + \phi s^2\partial_v^2\hat{Q}_0/2$, where \hat{Q}_2 remains to be found. Using relations analogous to those in Eq. (16) the result $\{s^2\}_2 = \{\hat{1}\}_2 + \partial_v^2\hat{Q}_0$ can be shown to hold also for the modulated quantities. This can be used, together with Eqs. (27) and (31), to derive the following two equations:

$$\hat{R}_2\delta(v - v_{re}) = i\omega\{s^2\}_2 + \partial_v\hat{J}_2 - i\omega\partial_v^2\hat{Q}_0, \quad (35)$$

$$\hat{J}_2 = (f - \partial_v)\{s^2\}_2 + \hat{\epsilon}\{s^2\}_2 \\ + (\partial_v\hat{Q}_0)(\partial_v f - 1 + i\omega) + \frac{\hat{R}_0}{\delta_T}\delta(v - v_{re}), \quad (36)$$

that together constitute the generalization of Eq. (17) to sinusoidal modulations. These simultaneous equations for $\{\hat{s}^2\}_2$ and \hat{J}_2 can be solved using the Threshold Integration scheme by resolving them into two subpairs: One pair proportional to \hat{R}_2 that takes care of the boundary conditions, and one pair that accounts for all inhomogeneous terms. Once these subsolutions have been derived a normalization condition can be applied to extract \hat{R}_2 (see the Appendix for details).

D. Limit of frozen fluctuations

The Fokker-Planck Eq. (29) in the limit $\kappa \rightarrow \infty$ is

$$i\omega\hat{P}_\infty + \partial_v[(s+f)\hat{P}_\infty + \hat{\epsilon}P_\infty] = (f\hat{P}_\infty)^{\text{th}}\delta(v-v_{\text{re}}). \quad (37)$$

The solutions can be separated into the form $\hat{P}_\infty(v,s) = \hat{P}_\infty(v|s)\phi(s)$, where $\hat{P}_\infty(v|s) = \hat{P}_{\text{det}}$ is the modulated density for the deterministic system with a constant current s with a rate $\hat{R}_{\text{det}} = (f\hat{P}_\infty(v|s))^{\text{th}}$. The total modulated rate therefore takes the form

$$\hat{R}_\infty = \int_{s_c}^{\infty} ds\phi(s)\hat{R}_{\text{det}}(s), \quad (38)$$

where s_c is the critical current below which the neuron does not fire. The interpretation of the homogeneous stochastic

population becoming identical to a heterogeneous deterministic population, in this limit, holds also for the firing-rate response. The deterministic rate modulation, from the solution of Eq. (37), is

$$\hat{R}_{\text{det}} = \frac{\hat{\epsilon} i\omega R_{\text{det}}}{e^{i\omega/R_{\text{det}}} - 1} \int_{v_{\text{re}}}^{\infty} \frac{dv}{(f+s)^2} \exp\left(i\omega \int_{v_{\text{re}}}^v \frac{dv}{f+s}\right). \quad (39)$$

This is the generalization to the EIF of the early result [20] for the leakless integrate-and-fire model. Note that the denominator vanishes when the modulation frequency is a multiple of the deterministic steady-state rate, leading to an infinite series of divergences in the deterministic rate response [see inset to Figs. 2(Ai–ii)].

E. Summary for the firing-rate response

The results for the rate modulation of a population of EIF neurons, receiving modulated current in the presence of filtered fluctuations, are summarized in Fig. 2. Figures 2(Ai) and 2(Aii) plot the amplitude of the firing-rate response as a function of the modulation frequency $\omega/2\pi$ for the suprathreshold (i) and subthreshold (ii) examples from Fig. 1. It is again striking how closely the white-noise [green lines, Eqs. (32) and (33)]

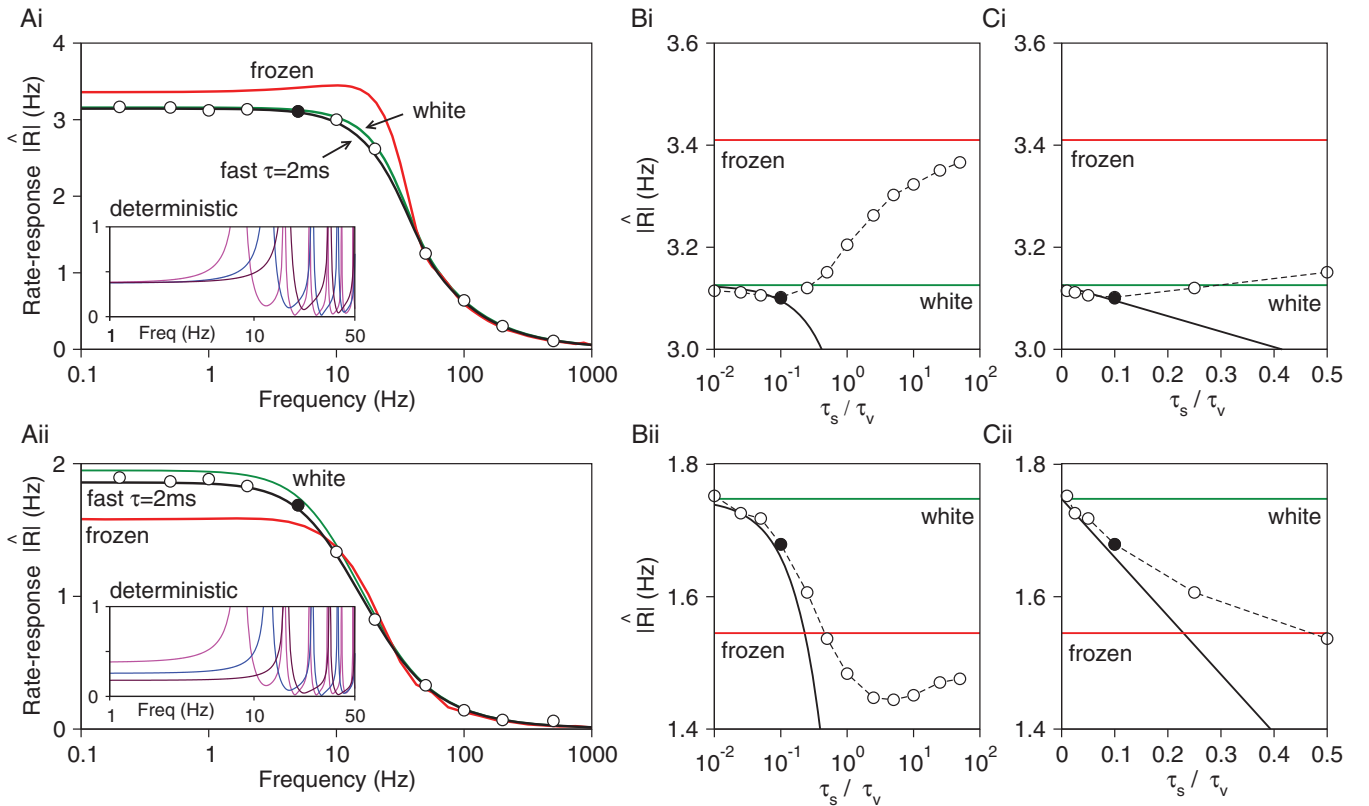


FIG. 2. (Color online) Firing-rate response of the EIF model subject to filtered noise. (Ai) Rate-modulation amplitude for the suprathreshold firing-regime example (i) from Fig. 1 showing the limits of white noise [green, Eqs. (32) and (33)] and frozen noise [red, Eq. (38)], and the fast-noise expansion $\hat{R}_0 + \kappa^2\hat{R}_2$ [black, Eqs. (35) and (36) for \hat{R}_2] for $\tau_s = 2$ ms compared to simulations (symbols). The inset shows three values of the integrand $\phi(s)\hat{R}_{\text{det}}$ in Eq. (38) with s corresponding to $E = -55, -54, -53$ mV (magenta, blue and indigo lines) for the Gaussians in Figs. 1(A) (Bi) and (Ci) Rate response at 5 Hz modulation for a range of filtering $\kappa^2 = \tau_s/\tau_v$ on logarithmic and linear scales for the suprathreshold case with the fast-noise expansion compared to simulations. (Aii–Cii) Same data but for the subthreshold example from Fig. 1. The modulation strength was $\hat{E} = 1$ mV with all other parameters provided in the caption to Fig. 1.

and frozen-noise [red lines, Eq. (38)] limits agree. At low modulation frequencies (<10 Hz) this similarity is a consequence of the close agreement for the steady state because the firing-rate response at low frequencies is proportional to the gradient of the steady-state rate dR/dE . At high frequencies (>100 Hz) the amplitude of the rate response is determined by the EIF spike dynamics [9] and converges to $R/i\omega\tau_v\Delta_T$, per unit modulation amplitude, regardless of the fluctuation time scale. This result can be rederived here from Eqs. (27) and (28), which yields $\{\hat{1}\} = -\hat{\epsilon}\partial_v\{1\}/i\omega$ in the large ω limit, and then using the large v results $R \simeq f\{1\}$ and $\hat{R} \simeq f\{\hat{1}\}$ from Eqs. (11) and (28). However, this result is less obvious when the case of frozen noise Eq. (38) is considered, which is equivalent to a heterogeneous network of deterministic neurons. The response of deterministic neurons to modulations Eq. (39) features divergences at multiples of the inverse period [see insets in Figs. 2(Ai)–(ii)], and hence the resulting smooth decay of $1/i\omega$, as argued from the Fokker-Planck equation, implies a cancellation of these divergences at multiple frequencies. The results of the fast-noise expansion $\hat{R}_0 + \kappa^2\hat{R}_2$ [black lines, Eqs. (35) and (36) for \hat{R}_2] are compared with simulations for filtered fluctuations ($\tau_s = 2$ ms) corresponding to fast AMPA synapses and shown to provide a good account for both suprathreshold and subthreshold examples. The quality of the fast-noise expansion is further examined in Figs. 2(B)–(Ci–ii) for a fixed modulation frequency of 5 Hz (chosen to be near that of theta rhythms seen in cortical and subcortical structures) over a range of filtering time constants $\kappa^2 = \tau_s/\tau_v$ showing a linear response at small τ_s , as expected by this second-order expansion. For the examples presented here, the variation in the modulated amplitude as a function of filtering time constant for a range spanning four orders of magnitude was small—less than 15%.

V. DISCUSSION

We have analyzed the firing dynamics of the EIF model subject to white, fast, or frozen fluctuations. Our results generalize previous analyses of the effects of filtered inputs on the steady-state rate of LIF [2,5,6] and QIF [8] neurons, and we extended the methodology further to examine the firing-rate dynamics under weak sinusoidally modulated afferent drive. A perturbative solution of the 1 + 2 dimensional Fokker-Planck equation allowed for the steady-state and firing-rate response to be derived analytically in a power series of the ratio of filtering to membrane time constants $\kappa = \sqrt{\tau_s/\tau_v}$, with the expansion to second-order agreeing well with simulations at the physiologically relevant time scale of excitatory AMPA synapses $\tau_s = 2$ ms.

However, taking a more broad view, a clear result of the study was the insensitivity of the firing rate to the time scale of filtering, if the amplitude of the fluctuations was varied so that the voltage distribution was more-or-less constant. The result is surprising given that the states of the populations are very different when subject to fast or frozen noise. For fast noise the population comprises homogeneous neurons firing stochastically, whereas for frozen noise the population is heterogeneous, featuring some silent neurons and others firing regularly with a distribution of fixed rates. That the low frequency of the firing-rate response was relatively similar

(less than 15% difference here between white and frozen cases for both subthreshold and suprathreshold regimes) is a consequence of the relation between the low-frequency rate response and the gradient of the steady-state rate versus resting potential curve. More remarkable is the agreement at high-frequency modulation. Though it has been shown from an analysis of the Fokker-Planck equation that any colored noise will lead to the same high-frequency asymptotics of $1/i\omega$ for the EIF [9], when taken to the extreme of frozen fluctuations this result asserts a complex cancellation of the divergent peaks in the response of the deterministic neurons comprising the population. It would be interesting to examine the nature of the cancellation of divergences for heterogeneous populations with non-Gaussian distributions of frozen noise for which asymptotics from a Fokker-Planck equation cannot be derived, but a result in terms of a distribution over deterministic neurons Eq. (38) can be derived.

Which neglected biophysical properties would be likely to disturb this similarity between homogeneous stochastic populations and heterogeneous deterministic populations? One feature of juvenile neocortical networks is short-term synaptic dynamics [21] such as depression or facilitation. These dynamics are sensitive to the temporal correlations in spike trains and, in the context of a recurrent network, would distinguish between fibers activated at the same typical rates but with different coefficients of variation, such as due to stochastic or deterministic presynaptic neurons. A second, intrinsic neuronal property, that has the potential to break the similarity between fast and frozen fluctuations is the effect of voltage-gated currents. For very slow voltage-gated currents it can be expected that, again, the voltage distribution is the key determinant of the level of activation [22]. However, rapidly activating currents such as the fast [23] or slower [24,25] components of the inactivation of the sodium spike-generating current are sensitive to the recent history of voltage dynamics near the action-potential threshold and have been shown to significantly impact the response properties of neurons *in vivo* [26]. It can be noted that the theoretical framework developed here provides a basis for future studies that aim to examine how EIF neurons with sodium-current inactivation [10,27] interact with filtered fluctuations at the level of populations and networks.

APPENDIX: THRESHOLD INTEGRATION

The linearity of the Fokker-Planck equation allows for an efficient numerical scheme to be employed to obtain the steady-state and linear-response solutions [13]. The method works by resolving the Fokker-Planck equation into the continuity and flux equations: two coupled first-order linear differential equations for the flux and density, respectively. These pairs of equations feature boundary conditions at the threshold and reset that are proportional to an *a priori* unknown ratelike quantity and may also feature inhomogeneous terms. The “trick” of the method is to separate the solution of these two equations into two additional pairs, one pair proportional to the unknown ratelike quantity that will account for the boundary conditions and one pair that accounts for the inhomogeneous terms. These two pairs of solutions are each obtained numerically by integrating backward from a threshold V_{th} to a lower bound V_{lb} . The resulting two pairs of solutions

are then linearly combined in such a way so as to ensure that probability is normalized, thereby fixing the unknown rate and solving the Fokker-Planck equation. The threshold and lower bound are chosen such that their values do not materially affect the final answer; the values used here were $V_{\text{th}} = 0$ mV and $V_{\text{lb}} = -100$ mV. The equations to be solved for each of the cases treated in this paper are first specified with a convenient numerical scheme provided at the end of the Appendix.

1. Zeroth-order steady-state solution

In this case the differential Eq. (14) can be solved analytically and the resulting integrals evaluated numerically; however, Threshold Integration provides a more direct route. There is no inhomogeneous term in (14), and so the substitution $Q_0 = R_0 Q_0^R$ is sufficient. The resulting differential equation for Q_0^R contains no unknowns and can be integrated backward from v_{th} down to the lower bound v_{lb} . The unknown rate R_0 is then extracted by the normalization condition on the probability density Q_0 , so that $R_0 = 1 / \int_{v_{\text{lb}}}^{v_{\text{th}}} dv Q_0^R$.

2. Second-order steady-state solution

Equation (17) for $\{s^2\}_2$ features a boundary term proportional to R_2 and two inhomogeneous terms. The solution is resolved into two parts $\{s^2\}_2 = R_2 \{s^2\}_2^R + \{s^2\}_2^I$, where $\{s^2\}_2^R$ and $\{s^2\}_2^I$ satisfy

$$(f - \partial_v) \{s^2\}_2^R = \theta(v - v_{\text{re}}), \quad (\text{A1})$$

$$(f - \partial_v) \{s^2\}_2^I = (1 - \partial_v f) \partial_v Q_0 - \frac{R_0}{\delta_T} \delta(v - v_{\text{re}}), \quad (\text{A2})$$

which are solved numerically by integrating from threshold to the lower bound v_{lb} . Because $\int dv \{s^2\} = 1$ it must be that $\int_{v_{\text{lb}}}^{v_{\text{th}}} dv \{s^2\}_2 = 0$, and so $R_2 = - \int_{v_{\text{lb}}}^{v_{\text{th}}} dv \{s^2\}_2^I / \int_{v_{\text{lb}}}^{v_{\text{th}}} dv \{s^2\}_2^R$, which in turn gives the combination of $\{s^2\}_2^R$ and $\{s^2\}_2^I$ required to form $\{s^2\}_2$.

3. Zeroth-order linear-response solution

The pair of Eqs. (32) and (33) for \hat{Q}_0 and \hat{J}_0 feature a boundary term proportional to the unknown \hat{R}_0 and an inhomogeneous term $\hat{\epsilon} Q_0$. Separating the solutions into rate and inhomogeneous terms $\hat{Q}_0 = \hat{R}_0 \hat{Q}_0^R + \hat{Q}_0^I$ and similarly for \hat{J}_0 gives two pairs of simultaneous differential equations to be solved by integrating down to the lower bound from threshold:

$$-\partial_v \hat{J}_0^R = i\omega \hat{Q}_0^R - \delta(v - v_{\text{re}}), \quad (\text{A3})$$

$$(f - \partial_v) \hat{Q}_0^R = \hat{J}_0^R, \quad (\text{A4})$$

and

$$-\partial_v \hat{J}_0^I = i\omega \hat{Q}_0^I, \quad (\text{A5})$$

$$(f - \partial_v) \hat{Q}_0^I = \hat{J}_0^I - \hat{\epsilon} Q_0. \quad (\text{A6})$$

The modulated flux $\hat{J}_0 = \hat{R}_0 \hat{J}_0^R + \hat{J}_0^I$ at sufficiently low voltages (at the lower bound, for example) must vanish, and hence $\hat{R}_0 = -\hat{J}_0^I(v_{\text{lb}}) / \hat{J}_0^R(v_{\text{lb}})$.

4. Second-order linear-response solution

Equations (35) and (36) can be solved using the same method used for the zeroth-order case by introducing $\{s^2\}_2 = \hat{R}_2 \{s^2\}_2^R + \{s^2\}_2^I$ and $\hat{J}_2 = \hat{R}_2 \hat{J}_2^R + \hat{J}_2^I$, which satisfy the two equation pairs

$$-\partial_v \hat{J}_2^R = i\omega \{s^2\}_2^R - \delta(v - v_{\text{re}}), \quad (\text{A7})$$

$$(f - \partial_v) \{s^2\}_2^R = \hat{J}_2^R, \quad (\text{A8})$$

and

$$-\partial_v \hat{J}_2^I = i\omega \{s^2\}_2^I - i\omega \partial_v^2 \hat{Q}_0, \quad (\text{A9})$$

$$(f - \partial_v) \{s^2\}_2^I = \hat{J}_2^I - \hat{\epsilon} \{s^2\}_2 + (\partial_v \hat{Q}_0)(1 - \partial_v f - i\omega) - \frac{\hat{R}_0}{\delta_T} \delta(v - v_{\text{re}}). \quad (\text{A10})$$

The modulated rate at second order is given by the ratio $\hat{R}_2 = -\hat{J}_2^I(v_{\text{lb}}) / \hat{J}_2^R(v_{\text{lb}})$.

5. Numerical implementation

Because of the exponentially large values of the function $f(v)$ at high voltages it is more convenient to use a slightly modified scheme rather than the standard Euler method for the integration of equations of the form

$$-(\partial_v X - fX) = H(v). \quad (\text{A11})$$

By partially integrating this equation between two voltage steps, the following form can be derived:

$$X_{k-1} = a_k X_k + \Delta b_k H_k$$

where

$$a_k = e^{-\Delta f_k} \quad \text{and} \quad b_k = \frac{1 - e^{-\Delta f_k}}{\Delta f_k}. \quad (\text{A12})$$

The voltage integration step is Δ , and the $k = 1 \dots n$ superscript implies evaluation at a particular voltage $v = v_k$ with $v_n = v_{\text{th}}$ at threshold and $v_1 = v_{\text{lb}}$ at the lower bound. The boundary conditions at threshold for scaled fluxlike quantities is $J^R(v_{\text{th}}) = 1$ and $J^I(v_{\text{th}}) = 0$, whereas the condition at threshold for quantities X that obey equations like (A12) are $X(v_{\text{th}}) \simeq H(v_{\text{th}}) / f(v_{\text{th}})$ because $fX \gg \partial_v X$.

- [1] N. Brunel and S. Sergi, *J. Theor. Biol.* **195**, 87 (1998).
 [2] N. Brunel, F. Chance, N. Fourcaud, and L. Abbott, *Phys. Rev. Lett.* **86**, 2186 (2001).
 [3] B. Lindner, *Phys. Rev. E* **69**, 022901 (2004).

- [4] J. W. Middleton, M. J. Chacron, B. Lindner, and A. Longtin, *Phys. Rev. E* **68**, 021920 (2003).
 [5] R. Moreno, J. de la Rocha, A. Renart, and N. Parga, *Phys. Rev. Lett.* **89**, 288101 (2002).

- [6] R. Moreno-Bote and N. Parga, *Phys. Rev. Lett.* **92**, 028102 (2004).
- [7] G. B. Ermentrout and N. Kopell, *SIAM J. Appl. Math.* **46**, 233 (1986).
- [8] N. Brunel and P. Latham, *Neural Comput.* **15**, 2281 (2003).
- [9] N. Fourcaud-Trocmé, D. Hansel, C. van Vreeswijk, and N. Brunel, *J. Neurosci.* **23**, 11628 (2003).
- [10] L. Badel, S. Lefort, R. Brette, C. C. H. Petersen, W. Gerstner, and M. J. E. Richardson, *J. Neurophysiol.* **99**, 656 (2008).
- [11] L. Badel, S. Lefort, T. K. Berger, C. C. H. Petersen, W. Gerstner, and M. J. E. Richardson, *Biol. Cybern.* **99**, 361 (2008).
- [12] B. Naundorf, F. Wolf, and M. Volgushev, *Nature (London)* **440**, 1060 (2006).
- [13] M. J. E. Richardson, *Phys. Rev. E* **76**, 021919 (2007).
- [14] A. Destexhe, M. Rudolph, J.-M. Fellous, and T. J. Sejnowski, *Neuroscience* **107**, 13 (2001).
- [15] M. J. E. Richardson and W. Gerstner, *Neural Comput.* **17**, 923 (2005).
- [16] H. Risken, *The Fokker-Planck Equation: Methods of Solution and Applications* (Springer, Berlin, 1989).
- [17] R. Moreno-Bote and N. Parga, *Neural Comput.* **22**, 1528 (2010).
- [18] N. Brunel and V. Hakim, *Neural Comput.* **11**, 1621 (1999).
- [19] N. Fourcaud-Trocmé and N. Brunel, *J. Comput. Neurosci.* **18**, 311 (2005).
- [20] B. W. Knight, *J. Gen. Physiol.* **59**, 734 (1972).
- [21] H. Markram, Y. Wang, and M. Tsodyks, *Proc. Natl. Acad. Sci. USA* **95**, 5323 (1998).
- [22] M. J. E. Richardson, *Phys. Rev. E* **80**, 021928 (2009).
- [23] A. L. Hodgkin and A. F. Huxley, *J. Physiol. Lond.* **117**, 500 (1952).
- [24] I. A. Fleidervish, A. Friedman, and M. J. Gutnick, *J. Physiol.* **493**, 83 (1996).
- [25] J. Benda and A. V. M. Herz, *Neural Comput.* **15**, 2523 (2003).
- [26] M. A. Farries, H. Kita, and C. J. Wilson, *J. Neurosci.* **30**, 13180 (2010).
- [27] J. Platkiewicz and R. Brette, *PLoS Comput. Biol.* **6**, e1000850 (2010).